UC San Diego
UC San Diego Previously Published Works

Title
Spontaneous transport barriers quench turbulent resistivity in two-dimensional magnetohydrodynamics

Permalink
https://escholarship.org/uc/item/9hw6h8kq

Journal
Physical Review E, 99(4)

ISSN
2470-0045

Authors
Fan, Xiang
Diamond, PH
Chacón, L

Publication Date
2019-04-01

DOI
10.1103/physreve.99.041201

Supplemental Material
https://escholarship.org/uc/item/9hw6h8kq#supplemental

Peer reviewed

Spontaneous transport barriers quench turbulent resistivity
in two-dimensional magnetohydrodynamics

Xiang Fan and P. H. Diamond
University of California at San Diego, La Jolla, California 92093, USA

L. Chacón
Los Alamos National Laboratory, Los Alamos, New Mexico 87545, USA

This Rapid Communication identifies the physical mechanism for the quench of turbulent resistivity in two-dimensional magnetohydrodynamics. Without an imposed, ordered magnetic field, a multiscale, blob-and-barrier structure of magnetic potential forms spontaneously. Magnetic energy is concentrated in thin, linear barriers, located at the interstices between blobs. The barriers quench the transport and kinematic decay of magnetic energy. The local transport bifurcation underlying barrier formation is linked to the inverse cascade of $\langle A^2 \rangle$ and negative resistivity, which induce local bistability. For small-scale forcing, spontaneous layering of the magnetic potential occurs, with barriers located at the interstices between layers. This structure is effectively a magnetic staircase.

I. INTRODUCTION

The evolution of mean quantities in turbulence is frequently modeled as a *transport process*, using ideas from the kinetic theory of gases. A classic example is that of Prandtl's theory of turbulent boundary layers, which first proposed the use of an eddy viscosity—based upon mixing length theory—to calculate mean flow profiles at a high Reynolds number. Magnetohydrodynamics (MHD) presents additional challenges, especially at high magnetic Reynolds number Rm. There, models based on transport theory concepts are central to our understanding of mean B ($\langle \mathbf{B} \rangle$) evolution in turbulent flows. Indeed, the well-known theory of mean-field electrodynamics (Moffatt [1]) employs transport coefficients α, β—related to turbulent helicity and energy, respectively—to describe the growth and transport of a mean magnetic field. Such models are heavily utilized in dynamo theory, the study of how large-scale fields are formed. The turbulent or "eddy" *resistivity* η_T is ubiquitous in these models (and corresponds to β above). While η_T is often taken as kinematic ($\eta_T \sim \eta_K \sim \sum_{\mathbf{k}} \langle \tilde{v}^2 \rangle_{\mathbf{k}} \tau_c$, where τ_c is the self-correlation time) for many applications, a nonlinear dependence of η_T on magnetic field and potential has been observed in numerous simulations [2–21]. Such nonlinearity arises from the fact that the magnetic fields alter the turbulent flows which scatter them. As this nonlinearity tends to reduce η_T relative to kinematic expectations, such trends are referred to as quenching. Rm-dependent quenching, i.e., when the product $\text{Rm}\langle \mathbf{B} \rangle^2$ enters, is of particular interest, as it signals that for the relevant case of high Rm, relatively weak fields can produce significant feedback on transport and evolution processes. Such Rm-dependent feedback has been associated with Alfvenization (i.e., the conversion of hydrodynamics turbulence to Alfven wave turbulence) and/or with the balance of magnetic helicity $\langle \mathbf{A} \cdot \mathbf{B} \rangle$ [i.e., in three dimensions (3D)] or $\langle A^2 \rangle$ [i.e., in two dimensions (2D)]. Both

arguments ultimately point to *memory*, due to the freezing-in law, as the origin of the quench. The quenching problem is also relevant to models of fast reconnection and impulsive energy release processes in MHD, as it constrains the size of (frequently invoked) anomalous dissipation [22,23]. More generally, it is an important paradigm of the transport of an active scalar.

In a seminal paper [2] which broached the quenching question, Cattaneo and Vainshtein (CV) presented numerical simulations of 2D MHD turbulence which demonstrated that even a weak large-scale magnetic field is sufficient to quench the turbulent transport of the active scalar A (the magnetic potential). Based on ideas from mean-field theory, CV suggested—and presented simulations to support—the idea that η_T is given by

$$\eta_T \sim \frac{\langle v^2 \rangle^{1/2} l}{1 + \frac{1}{\mu_0 \rho} \text{Rm}\langle \mathbf{B} \rangle^2 / \langle v^2 \rangle}. \quad (1)$$

The mean field $\langle \mathbf{B} \rangle$ here is estimated using

$$|\langle \mathbf{B} \rangle| \sim \sqrt{\langle A^2 \rangle} / L_0, \quad (2)$$

where L_0 is system size. For $\frac{1}{\mu_0 \rho} \text{Rm}\langle \mathbf{B} \rangle^2 / \langle v^2 \rangle < 1$, $\eta_T \sim \eta_K \sim \langle v^2 \rangle^{1/2} l$, while for $\frac{1}{\mu_0 \rho} \text{Rm}\langle \mathbf{B} \rangle^2 / \langle v^2 \rangle > 1$, $\eta_T \ll \eta_K$, so η_T is quenched. It is important to note that, in view of Cowling's theorem, suppression occurs only for a time of *limited duration*, without external forcing of A. After the aforementioned suppression stage, a rapid decay of the magnetic field occurs, and η_T reverts to η_K. The evolutions of E_B, E_K (magnetic and kinetic energy) and $\langle A^2 \rangle$ (mean-square potential) are shown in Figs. 1(a) and 1(b).

Equation (1) was also obtained analytically from statistical theory, assuming the presence of an imposed weak large-scale field $\mathbf{B}_0$ (i.e., $\langle \mathbf{B} \rangle = \mathbf{B}_0$) [24–27]. (Note the assumptions that
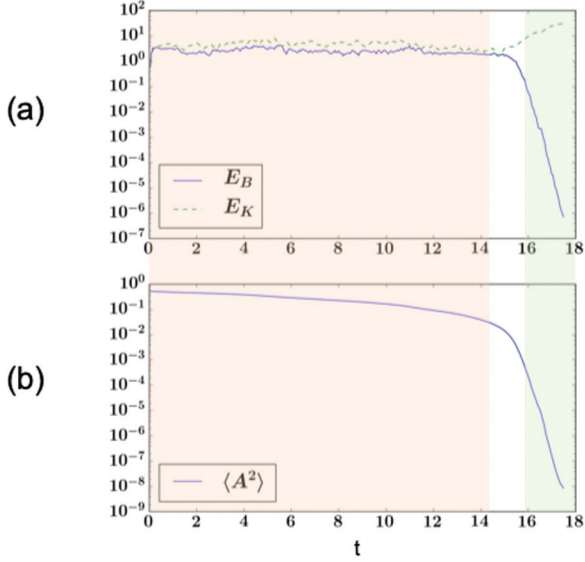
FIG. 1. Time evolution of (a) magnetic energy E_B and kinetic energy E_K; (b) $\langle A^2 \rangle$ in run 1. The suppression stage is marked in orange, and the kinematic decay stage in green. The decay of E_B is slow in the suppression stage, which is consistent with previous studies. The decay of $\langle A^2 \rangle$ is also slow in the suppression stage, and is more smooth compared to E_B.

$|\langle \mathbf{B} \rangle|$ is determined by root-mean-square A and the system size in CV.) The derivation made use of $\langle A^2 \rangle$ balance to constrain the turbulent resistivity [28–30]. Rm dependence of the quench stems from the fact that $\langle A^2 \rangle$ is conserved up to resistive diffusion. This early work on resistivity quenching triggered a tidal wave of subsequent studies of nonlinear dynamo evolution and quenching.

In this Rapid Communication, we show that, without an imposed, ordered magnetic field, Rm-dependent quenching is intrinsically an intermittency phenomena, and can occur where a global mean field $\langle \mathbf{B} \rangle$ simply does not exist. Rather, turbulent resistivity quenching occurs due to intermittent *transport barriers*. A transport barrier is a localized region of mixing and transport significantly lower than the mean thereof, i.e., $\eta_{T,\text{local}} < \bar{\eta}_T$. These barriers are extended, thin, linear features, into which strong $\langle B^2 \rangle$ is concentrated. The barriers are formed by the $\langle B^2 \rangle$ feedback on scalar transport, specifically by magnetic flux coalescence. Thus, transport quenching is manifestly not a mean-field effect, as the structure of the field is more akin to a random network than to a smooth mean field. The barriers form in the interstices between blobs of $\langle A^2 \rangle$, which are formed by the inverse cascade of $\langle A^2 \rangle$. Overall, the magnetic potential and field have a structure of "blob-and-barrier" at large Rm, as shown in Fig. 2. In contrast to the assumptions of CV, the magnetic field exhibits *two* nontrivial scales, i.e., the blob size L_{blob} and the barrier width W, where $W \ll L_{\text{blob}}$. L_{blob} characterizes the magnetic potential while W characterizes the field intensity.

The A field in the blob-and-barrier structure of 2D MHD resembles the concentration contrast field ψ in the Cahn-Hilliard Navier-Stokes (CHNS) system [31–35]. The CHNS and 2D MHD systems are compared in the Supplemental Material [36].

TABLE I. Initial conditions, k, and Rm for the suppression stage. For all runs, $A_0 = 1.0$ and $f_0 = 30$.

Runs	Initial condition	η	ν	$1/(\mu_0\rho)$	k	Rm
Run 1	Bimodal	1×10^{-4}	1×10^{-4}	0.04	5	~500
Run 2	Unimodal	1×10^{-4}	1×10^{-4}	0.04	5	~500
Run 3	Bimodal	1×10^{-4}	2×10^{-3}	0.01	32	~150

II. ANALYSIS: GLOBAL

In this Rapid Communication, the 2D MHD equations are solved using direct numerical simulation [37,38] with a doubly periodic boundary condition,

$$\partial_t A + \mathbf{v} \cdot \nabla A = \eta \nabla^2 A, \tag{3}$$

$$\partial_t \omega + \mathbf{v} \cdot \nabla \omega = \frac{1}{\mu_0\rho}\mathbf{B} \cdot \nabla \nabla^2 A + \nu \nabla^2 \omega + f. \tag{4}$$

Here, ω is the vorticity, η is the resistivity, ν is the viscosity, $\mu_0\rho$ is the magnetic permeability and density, and f is an isotropic homogeneous external forcing, with wave number k and magnitude f_0. The simulation box size is $L_0^2 = 1.0 \times 1.0$ with 1024×1024 resolution. The parameters used are summarized in Table I. The initial condition for the ω field is $\omega_I = 0$ everywhere; the initial condition for A field is a cosine function in run 1: $A_I(x, y) = A_0 \cos 2\pi x$. The setup of run 1 differs from that of Ref. [2] only in the range of Rm studied.

A nontrivial blob-and-barrier structure is observed in real space at large Rm, and this structure forms quickly after a short transition period. Figure 2(a1) shows a snapshot of magnetic potential in the suppression stage for run 1. It consists of "blobs" (regions in red and blue) and interstices (green), and is very different from the initial condition, for which a mean field is relevant. Figure 2(a2) shows the B^2 field for the same run. The high B^2 regions (bright color) occur at the interstices of the A blobs, since $\mathbf{B} \equiv \hat{\mathbf{z}} \times \nabla A$. The interstices have a one-dimensional shape. We call these one-dimensional, high B^2 regions "barriers," because these are the regions where transport is strongly suppressed relative to the kinematic case η_K, due to locally strong B^2, as discussed below. One measure of this blob-and-barrier structure is the structure of the probability density function (PDF) of A. As is shown in Fig. 2(a3), the PDF of A for run 1 during the suppression stage has two peaks, both at $A \neq 0$. Notably, such a structure of the PDF also appears in the analogous CHNS system. In comparison, in the kinematic decay stage of run 1 (i.e., at a later time, when the magnetic field is so weak that η_T reverts to η_K), the fields are well mixed and a nontrivial real-space structure is absent. No barriers are discernible in the decay stage. The corresponding PDF of A is a distribution for a passive scalar, with *one peak* at $A = 0$, as shown in Fig. 2, column (b). The time evolution of PDF of A for run 1 [Fig. 3(a)] has a horizontal Y shape. The PDF has two peaks initially, and the interval between the peaks decreases as the A field decays. The PDF changes from a double peak to a single peak as the system evolves from the suppression stage to the kinematic stage.
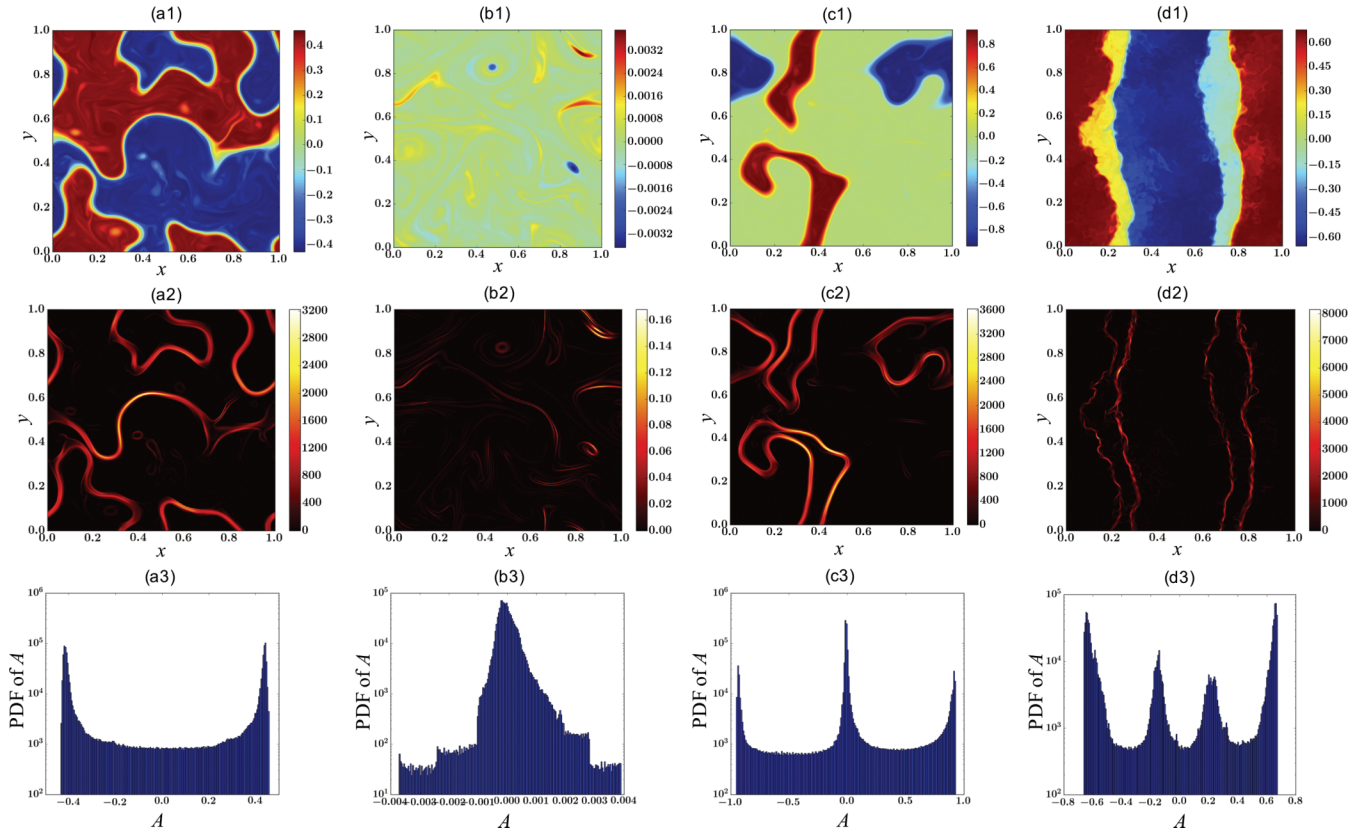
FIG. 2. Row 1: A field snapshots; row 2: B^2 field snapshots; row 3: PDF of A. Column (a): Run 1 at $t = 10$ (suppression stage). The system exhibits a blob-and-barrier feature, and the PDF of A is bimodal. Column (b): Run 1 at $t = 17$ (kinematic decay stage). The distribution of the fields is trivial. Column (c): Run 2 at $t = 10$. Two peaks still arise on the PDF of A even though its initial condition is unimodal. Column (d): Run 3 at $t = 4.5$. The system exhibits a staircase feature, and the PDF of A has multiple peaks.

Two quantities which characterize the field structure in the suppression stage are the *packing fraction P*, and *barrier width W*, defined below. In order to identify the barriers, we set a threshold on the local field intensity, and define the barriers to be the regions where $B(x, y) > \sqrt{\langle B^2 \rangle} * 2$. The packing fraction P is defined as

$$P \equiv \frac{\text{No. of grid points in barrier regions}}{\text{No. of total grid points}}. \quad (5)$$

P is the fraction of the space where the intensity exceeds the mean-square value. The expression for the barrier width is $W \sim \Delta A / B_b$, where ΔA is the difference in A between adjacent blobs, and B_b is the magnitude of the magnetic field in the barrier regions. We use $\sqrt{\langle A^2 \rangle}$ to estimate ΔA for the bimodal PDF, such as for run 1. The narrow barriers contain most of the magnetic energy. For example, in run 1 at $t = 10$, the barriers occupy only $P = 9.9\%$ of the system space, but
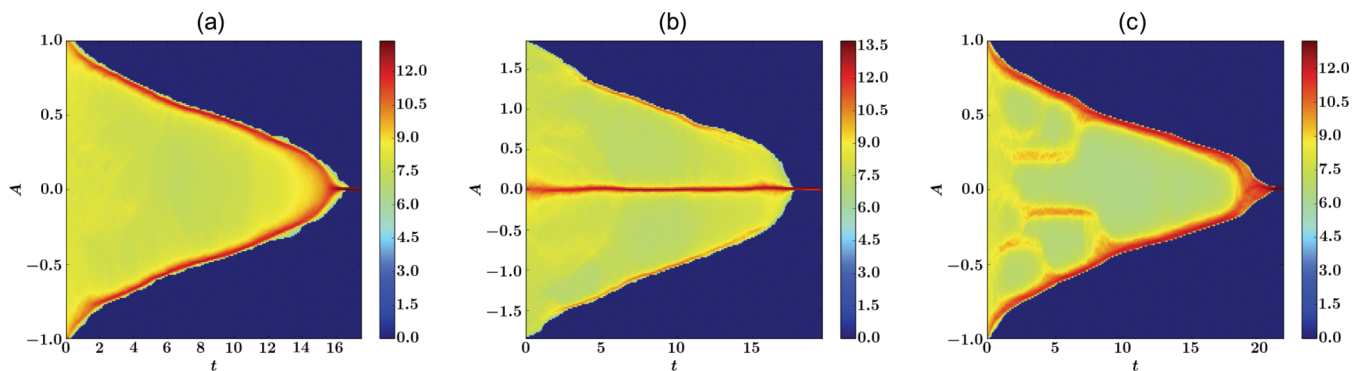

FIG. 3. The time evolutions of PDF of A, and the values are in logarithm scale (base 10). (a) For run 1, the PDF is bimodal in the suppression stage, and ΔA between the two peaks reduces in time. The PDF becomes unimodal in the kinematic decay stage. (b) For run 2, two peaks at $A \neq 0$ still arise spontaneously given a unimodal initial condition. (c) For run 3, with external forcing at a smaller scale, layering and coarsening can occur. See further explanations in the text.
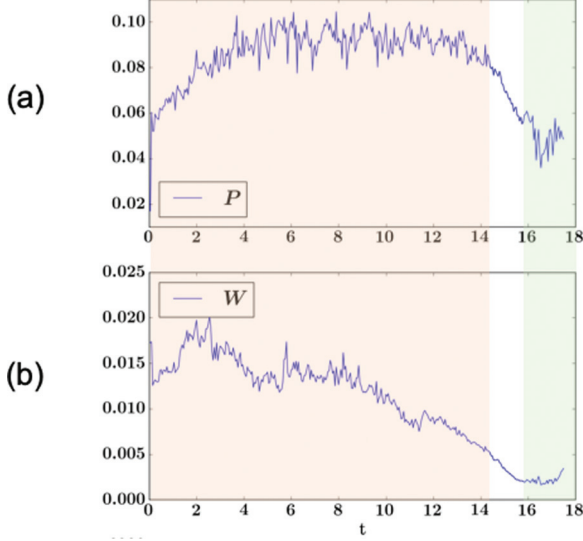
FIG. 4. Time evolution of (a) packing fraction P, and (b) barrier width W in run 1.

the magnetic field in these regions accounts for 80.7% of the magnetic energy. Therefore, we can use the magnetic energy in the barriers $\langle B_b^2 \rangle$ to approximate the total magnetic energy, i.e.,

$$\sum_{\text{barriers}} B_b^2 \sim \int d^2x B^2. \tag{6}$$

It follows that $\langle B_b^2 \rangle \sim \langle B^2 \rangle / P$. We can thus define W based on the arguments above as

$$W^2 \equiv \langle A^2 \rangle / (\langle B^2 \rangle / P). \tag{7}$$

This definition of W can be justified by measuring the approximate barrier widths. The time evolutions of P and W in run 1 are shown in Fig. 4. P stays at 0.08–0.10 throughout the suppression stage. P starts to decline near the end of the suppression stage, and drops to the noise level in the kinematic decay stage. W decreases during the suppression stage, due mainly to the decrease in ΔA. It is important to note that the decline in P, which begins at $t \sim 13$, slightly *leads* the decay in magnetic energy, which begins at $t \sim 15$. This supports the notion that barriers, the population of which is measured by P, are responsible for the quenching of mixing and decay in the suppression stage.

One may question whether the bimodal PDF is due to the initial condition, since the cosine initial condition in run 1 is bimodal. The answer is no. In order to show this, a unimodal initial condition is constructed for run 2, such that the initial PDF of A has one peak at $A = 0$ (see Supplemental Material [36] for details). Figure 2, column (c) shows a snapshot for run 2 at $t = 10$. The time evolution of the PDF of A for that case is shown in Fig. 3(b). It is evident that two nonzero peaks in the PDF of A still arise, even if the initial condition is unimodal. The blob structure in A and the barrier structure in B^2 are also evident.

III. ANALYSIS: LOCAL

One can easily see from the B^2 fields plots in Fig. 2 that a large-scale $\langle \mathbf{B} \rangle$ does not exist. Intermittent magnetic intensity, with low P, is a consequence of the blob-and-barrier structure. Therefore, the traditional approach of mean-field theory, especially Eq. (2), is neither applicable nor relevant. Globally, no theory exists for $\mathbf{B}_0 = \mathbf{0}$. Usual closure approaches appear useful when the averaging window is restricted to a suitable size, corresponding to a *localized region* within which a mean $\mathbf{B}$ exists. In order to derive an expression for the effective η_T for such a local region from dynamics, we extend the theory by Refs. [24–27], and propose

$$\eta_T = \frac{\langle v^2 \rangle^{1/2} l}{1 + \text{Rm} \frac{1}{\mu_0 \rho} \langle \mathbf{B} \rangle^2 / \langle v^2 \rangle + \text{Rm} \frac{1}{\mu_0 \rho} \frac{\langle A^2 \rangle}{L_{\text{blob}}^2} / \langle v^2 \rangle}. \tag{8}$$

Here, L_{blob} is the size of the large A blobs, i.e., the characteristic length scale for $\langle A^2 \rangle$. The derivation is shown below.

We start from

$$\frac{1}{2} [\partial_t \langle A^2 \rangle + \langle \nabla \cdot (\mathbf{v} A^2) \rangle] = -\Gamma_A \frac{\partial \langle A \rangle}{\partial x} - \eta \langle B^2 \rangle, \tag{9}$$

where $\Gamma_A = \langle v_x A \rangle$ is the spatial flux of A. In the past, only the $\Gamma_A \frac{\partial \langle A \rangle}{\partial x}$ term is kept in (9) to balance $\eta \langle B^2 \rangle$. However, in the absence of $\mathbf{B}_0$, $\Gamma_A \frac{\partial \langle A \rangle}{\partial x}$ term can be small, while the triplet term $\langle \nabla \cdot (\mathbf{v} A^2) \rangle$ can remain, if the average is taken over a window smaller than the system size L_0. Note the relevant scale l here is

$$l_d < W < l < L_0, \tag{10}$$

where l_d is the dissipation scale. Retaining all contributions, we have

$$\partial_t \langle A^2 \rangle = -\langle \mathbf{v} A \rangle \cdot \nabla \langle A \rangle - \nabla \cdot \langle \mathbf{v} A^2 \rangle - \eta \langle B^2 \rangle. \tag{11}$$

Now assume the fluxes are Fickian. Note that, in principle, there are two diffusion coefficients,

$$\langle \mathbf{v} A \rangle = -\eta_{T1} \nabla \langle A \rangle, \tag{12}$$

$$\langle \mathbf{v} A^2 \rangle = -\eta_{T2} \nabla \langle A^2 \rangle. \tag{13}$$

Plugging them in, we get

$$\partial_t \langle A^2 \rangle = \eta_{T1} (\nabla \langle A \rangle)^2 + \nabla \eta_{T2} \cdot \nabla \langle A^2 \rangle - \eta \langle B^2 \rangle. \tag{14}$$

The first term on the right-hand side is the turbulent diffusion of $\langle A \rangle$, corresponding to the large-scale magnetic field. The second term is the turbulent diffusion of $\langle A^2 \rangle$, which controls decay in a weak magnetic field. The third term is the usual collisional dissipation. In principle, $\eta_{T1} \neq \eta_{T2}$, though these two are related. Both terms are retained. For simplicity, we assume $\eta_{T1} = \eta_{T2} = \eta_T$. For a stationary state, we have

$$\langle B^2 \rangle \sim \frac{\eta_T}{\eta} \left(\langle B \rangle^2 + \langle A^2 \rangle / L_{\text{blob}}^2 \right), \tag{15}$$

where L_{blob} is the blob size, the characteristic length scale for $\langle A^2 \rangle$. By standard closure methods, one can obtain an expression for η_T [29,30],

$$\eta_T = \sum_{\mathbf{k}} \tau_c \left[\langle v^2 \rangle_{\mathbf{k}} - \frac{1}{\mu_0 \rho} \langle B^2 \rangle_{\mathbf{k}} \right]. \tag{16}$$
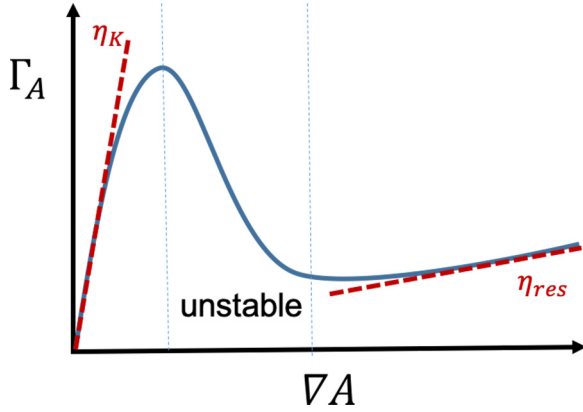
FIG. 5. A sketch showing the relationship between flux Γ_A and ∇A. The total resistivity is $\eta_{\text{tot}} = \delta\Gamma_A/\delta\nabla A$, and is composed of turbulent and collisional parts $\eta_{\text{tot}} = \eta_T + \eta$. In the small B limit, $\eta_{\text{tot}} \sim \eta_K$; in the large B limit, the residual resistivity is $\eta_{\text{res}} \sim \frac{ul}{\text{Rm}\frac{1}{\mu_0\rho}\langle B\rangle^2/\langle v^2\rangle + \text{Rm}\frac{1}{\mu_0\rho}\frac{\langle A^2\rangle}{L_{\text{blob}}^2}/\langle v^2\rangle} + \eta$. The transition between the two limits is the transport bifurcation.

Plugging (15) into (16) yields Eq. (8) proposed above. Detailed comparisons of Eq. (8) with simulation results are nontrivial and will be left for future work.

Note that $L_{\text{blob}} \ll L_0$. In regions where no high-intensity magnetic field is present, i.e., inside blobs, $\text{Rm}\frac{1}{\mu_0\rho}\langle B\rangle^2/\langle v^2\rangle$ is negligible. Yet transport is still reduced relative to kinematics by $\langle A^2\rangle$, via the $\text{Rm}\frac{1}{\mu_0\rho}\frac{\langle A^2\rangle}{L_{\text{blob}}^2}/\langle v^2\rangle$ term. In the barrier regions where the magnetic energy is large, $\text{Rm}\frac{1}{\mu_0\rho}\langle B\rangle^2/\langle v^2\rangle$ is dominant, since $\langle B^2\rangle \gg \langle A^2\rangle/L_{\text{blob}}^2$ for $P \ll 1$. Such regions—barriers—are where turbulent transport of A is most strongly suppressed.

A key question concerns how transport barriers form spontaneously in turbulent 2D MHD. We argue that transport barriers result from negative resistivity, driven by the inverse cascade of $\langle A^2\rangle$. In Eq. (16), the positive contribution to η_T is a consequence of turbulent mixing by fluid advection, while the second, negative, term is a consequence of flux coalescence. From the above, we see that the turbulent resistivity can go negative locally, where $\langle B^2\rangle$ is strong. Of course, the system-averaged resistivity is positive, so the field decays, though slowly. Note though that a local negative contribution can trigger a feedback loop, i.e., B^2 strong in a specific region $\rightarrow$ local η_T negative $\rightarrow$ local ∇A increases $\rightarrow$ local B^2 increases further. The feedback process saturates after the short transition period, as the inverse cascade of $\langle A^2\rangle$ must ultimately deplete the small scales.

Another way to view this evolution is as a local transport bifurcation—see the spatially local S-shaped flux-gradient curve for A, shown in Fig. 5 for illustration, which follows from Eq. (8). The S curve describes a bistable system. Note there are two stable ranges with positive slope, and one unstable region between, with a negative slope (as for negative resistivity). This implies that the barrier formation is a transport bifurcation, which occurs when the local magnetic intensity exceeds the threshold given by (16). This mechanism resembles a transport bifurcation in magnetically confined

systems [39,40]. Here, feedback via regions of locally intense B^2, rather than $\mathbf{E} \times \mathbf{B}$ shear, is the trigger for barrier formation.

IV. LAYERING OF MAGNETIC POTENTIAL

Inhomogeneous mixing and bistability (of which negative viscosity is a symptom) are the key elements in the dynamics of layering (i.e., staircase formation) in many systems [6,39,40]. Given that, and the ubiquitous blob-and-barrier structure here, it is natural to ask if spontaneous layering can occur in 2D MHD. We answer in the affirmative—see Fig. 2, column (d). The initial condition in run 3 is the same bimodal one as for run 1. The key difference in parameters is the forcing scale, which is smaller here, i.e., $k = 32$ in run 3, rather than $k = 5$ for the other runs. As shown in Fig. 3(c), the layered structure consists of regions of homogenized A, with small transition layers of sharp gradients in A (and thus B^2) between them. Layering thus induces transport barriers. The layered structure persists for the duration of the suppression stage, but coarsens, as shown in Fig. 3(c). Coarsening occurs by a sequence of blob mergers. Note that by $t \sim 4$ the staircase has coarsened to four transition layers. We note that closure theory for the evolution of $\langle A^2\rangle_{\mathbf{k}}$ predicts a positive turbulent hyperresistivity along with the negative component of the turbulent resistivity [26,27]. This implies that the evolution equation for mean $\langle A\rangle$ has a structure much as the Cahn-Hilliard equation, the solutions of which are known to manifest mergers and coarsening [34].

V. CONCLUSIONS

In summary, we observe a blob-and-barrier real-space structure in the decay of magnetic fields in turbulent 2D MHD. The magnetic field and the resulting barriers are highly intermittent, and cannot be treated by mean-field theory. The turbulent resistivity is suppressed in the barriers, where the magnetic fields are strong. The barriers form at blob interstices. For small-scale forcing, spontaneous layering of the magnetic potential occurs due to inhomogeneous mixing. Barriers form between layers. The layered structure coarsens in time.

This analysis has implications beyond 2D. One line of development is to the quenching of transport of magnetic helicity and magnetic dynamo processes by spatially intermittent but locally strong magnetic fields. The other is to anomalous dissipation in anisotropically ordered 3D systems, such as reduced MHD, where the nonlinear dynamics are effectively two dimensional. These topics will be pursued in the future.

[1] H. K. Moffatt, *Magnetic Field Generation in Electrically Conducting Fluids* (Cambridge University Press, Cambridge, UK, 1983).

[2] F. Cattaneo and S. I. Vainshtein, Astrophys. J., Lett. **376**, L21 (1991).

[3] S. I. Vainshtein and R. Rosner, Astrophys. J. **376**, 199 (1991).

[4] S. I. Vainshtein and F. Cattaneo, Astrophys. J. **393**, 165 (1992).

[5] F. Cattaneo, Astrophys. J. **434**, 200 (1994).

[6] N. J. Balmforth, S. G. L. Smith, and W. R. Young, J. Fluid Mech. **355**, 329 (1998).

[7] A. Lazarian and E. T. Vishniac, Astrophys. J. **517**, 700 (1999).

[8] D. Biskamp and E. Schwarz, Phys. Plasmas **8**, 3282 (2001).

[9] G. B. Field and E. G. Blackman, Astrophys. J. **572**, 685 (2002).

[10] P. D. Mininni, D. C. Montgomery, and A. G. Pouquet, Phys. Fluids **17**, 035112 (2005).

[11] E.-j. Kim, Phys. Rev. Lett. **96**, 084504 (2006).

[12] L. J. Silvers, Phys. Lett. A **334**, 400 (2005).

[13] L. J. Silvers, Mon. Not. R. Astron. Soc. **367**, 1155 (2006).

[14] N. Kleeorin and I. Rogachevskii, Phys. Rev. E **75**, 066315 (2007).

[15] S. R. Keating and P. H. Diamond, Phys. Rev. Lett. **99**, 224502 (2007).

[16] S. R. Keating, L. J. Silvers, and P. H. Diamond, Astrophys. J., Lett. **678**, L137 (2008).

[17] S. R. Keating and P. H. Diamond, J. Fluid Mech. **595**, 173 (2008).

[18] S. M. Tobias, P. H. Diamond, and D. W. Hughes, Astrophys. J., Lett. **667**, L113 (2007).

[19] G. L. Eyink, A. Lazarian, and E. T. Vishniac, Astrophys. J. **743**, 51 (2011).

[20] T. Kondić, D. W. Hughes, and S. M. Tobias, Astrophys. J. **823**, 111 (2016).

[21] J. Mak, S. D. Griffiths, and D. W. Hughes, Phys. Rev. Fluids **2**, 113701 (2017).

[22] P. W. Xi, X. Q. Xu, and P. H. Diamond, Phys. Rev. Lett. **112**, 085001 (2014).

[23] P. W. Xi, X. Q. Xu, and P. H. Diamond, Phys. Plasmas **21**, 056110 (2014).

[24] A. V. Gruzinov and P. H. Diamond, Phys. Rev. Lett. **72**, 1651 (1994).

[25] A. V. Gruzinov and P. H. Diamond, Phys. Plasmas **3**, 1853 (1996).

[26] P. H. Diamond, E. J. Kim, and D. W. Hughes, in *Fluid Dynamics and Dynamos in Astrophysics and Geophysics* (CRC Press, Boca Raton, FL, 2005), p. 145.

[27] P. H. Diamond, S.-I. Itoh, and K. Itoh, *Modern Plasma Physics, Vol. 1: Physical Kinetics of Turbulence Plasmas* (Cambridge University Press, Cambridge, UK, 2010).

[28] Y. B. Zeldovich, Sov. Phys. JETP **4**, 460 (1957).

[29] A. Pouquet, U. Frisch, and J. Léorat, J. Fluid Mech. **77**, 321 (1976).

[30] A. Pouquet, J. Fluid Mech. **88**, 1 (1978).

[31] R. Ruiz and D. R. Nelson, Phys. Rev. A **23**, 3224 (1981).

[32] X. Fan, P. H. Diamond, L. Chacón, and H. Li, Phys. Rev. Fluids **1**, 054403 (2016).

[33] X. Fan, P. H. Diamond, and L. Chacón, Phys. Rev. E **96**, 041101(R) (2017).

[34] X. Fan, P. H. Diamond, and L. Chacón, Phys. Plasmas **25**, 055702 (2018).

[35] R. Pandit, D. Banerjee, A. Bhatnagar, M. Brachet, A. Gupta, D. Mitra, N. Pal, P. Perlekar, S. S. Ray, V. Shukla, and D. Vincenzi, Phys. Fluids **29**, 111112 (2017).

[36] See Supplemental Material at http://link.aps.org/supplemental/10.1103/PhysRevE.99.041201 for details about the unimodal initial condition used in the main text, and the relationship between the CHNS system and MHD.

[37] L. Chacon, D. Knoll, and J. Finn, J. Comput. Phys. **178**, 15 (2002).

[38] L. Chacon and D. Knoll, J. Comput. Phys. **188**, 573 (2003).

[39] A. Ashourvan and P. H. Diamond, Phys. Rev. E **94**, 051202(R) (2016).

[40] A. Ashourvan and P. H. Diamond, Phys. Plasmas **24**, 012305 (2017).